J Mol Model (2017) 23:336
https://doi.org/10.1007/s00894-017-3509-3

ORIGINAL PAPER

Electronic properties of the polypyrrole-dopant anions ClO_4^- and MoO_4^{2-}: a density functional theory study

Nguyen Ngoc Ha[1] · **Ngo Tuan Cuong**[1] · **Hoang Van Hung**[1] · **Ha Manh Hung**[2] · **Vu Quoc Trung**[1]

Received: 4 July 2017 / Accepted: 24 October 2017

Abstract The conductive properties of polypyrrole chains doped with ClO_4^- or MoO_4^{2-} anions and the existence of polarons and bipolarons in these doped polypyrrole chains were investigated by performing computational calculations based on density functional theory (DFT). Doping with these anions was found to decrease the band gap of the polypyrrole. Theoretical calculations revealed that changing the type of oxidative agent applied does not affect the conversion of polypyrrole into a conducting polymer, but the conductivity of the doped polypyrrole does depend on the ratio of oxidant to polypyrrole.

Keywords DFT method · Polypyrroles · Polaron · Bipolaron · IR spectra

Introduction

Polypyrrole (PPy), an amorphous polymeric material (for the simplified structure of PPy, see Fig. 1), is currently being extensively researched because of its high electrical conductivity and durability. It can be easily synthesized by chemical and electrochemical methods from pyrrole monomers in various organic solvents or even in aqueous solutions [1–6]. The high electrical conductivity of PPy derives from its conjugated pyrrole rings. These pyrrole rings can be oxidized to become positively charged and to interact with different anions during doping, which significantly reduces the energy band gap of the material. This oxidation can be accomplished electrochemically (by immersing electrodes in pyrrole and then applying a voltage between the electrodes) or chemically (by applying various oxidizing agents such as iron(III) chloride, iron(III) perchlorate, ammonium peroxydisulfate, and many other substances) [2]. It is known that the removal of a π electron due to the oxidation of a polymer backbone generates a polaron (an interacting electron–hole pair), and that removing a second electron in a similar manner induces two polarons or one bipolaron. A bipolaron usually encompasses 1–6 carbon atoms and is associated with a structural deformation. Polarons and bipolarons are responsible for electrical conduction in polymer chains as they are mobile in an external electrical field [7–9].

Modifying PPys as described above can generate ecofriendly anticorrosive materials. The anticorrosive properties of modified PPys depend on the nature of the counter anions present, the properties of the solvent used, and the temperature applied [10, 11]. PPy-based materials are employed in rechargeable batteries [12, 13], sensors [14, 15], supercapacitors [16, 17], electromagnetic shielding [18, 19], and for corrosion protection [20, 21]. Notable among the various corrosion-resistant doped PPys is PPy doped with molybdate compensation anions; the mechanism for the corrosion resistance of this doped PPy has been investigated experimentally [22–25]. Although numerous experimental studies of PPy have been performed over the years, including research into their surface properties, theoretical studies of PPy using quantum chemical calculations remain scarce. A literature review indicated that theoretical investigations of PPy have mostly been implemented with low-level ab initio methods. For example, Ford and his colleagues used the semi-empirical method CNDO/S3 to analyze the UV-Vis

✉ Vu Quoc Trung
trungvq@hnue.edu.vn

[1] Faculty of Chemistry, Hanoi National University of Education, 136 Xuan Thuy Road, Cau Giay District, Hanoi, Vietnam

[2] Faculty of Basic Sciences, Hanoi University of Mining and Geology, 18 Vien Street, Duc Thang Ward, Bac Tu Liem District, Hanoi, Vietnam

Published online: 08 November 2017

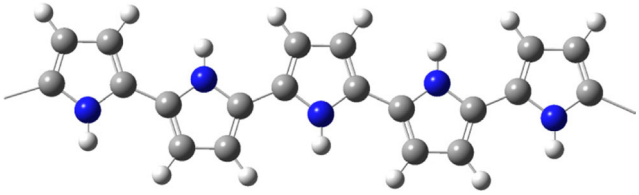

Fig. 1 Structure of polypyrrole (PPy), as drawn using the GaussView software package. The *small light-gray balls* represent H atoms, the *darker-gray balls* represent C atoms, and the *blue balls* represent N atoms

photoabsorption and emission of polypyrrole [11]. Their results suggested that an excited pyrrole cation could comprise as many as 4–6 pyrrole units. In another work, Bredas et al. explored the quarter pyrrole system with and without Na dopant using the Hartree–Fock method and the STO-3G basis set [26]. However, those calculation methods were not sufficient to achieve an accurate description of the electronic structure of polypyrrole.

Recently, density functional theory (DFT) has been emerged as a popular theoretical approach for studying the structures and properties of materials ranging from simple organic and inorganic compounds to conductive polymers [27–34]. For example, it has been applied to study the electronic properties of negatively charged *n*-pyrrole oligomers (n = 2–18) [35] and PPy [36]. In those studies, the band gaps and the conductivities of *n*Py and *n*Py-X (n = 1–9 and X = +, NH_3, or Cl) were investigated and the calculated infrared (IR) spectra of the substances were observed to fit well to the corresponding experimentally obtained IR spectra. DFT and time-dependent density functional theory (TD-DFT) methods have also been applied to calculate the electronic spectra of aniline and pyrrole monomers/dimers, which were again found to agree well with corresponding experimentally determined optical absorption spectra [37]. These methods have also been used to study the structures and properties of polyaniline [38–40] and polythiophenes [41–43].

It is known that PPys doped with MoO_4^{2-} or ClO_4^- anions have the potential to protect mild steel from corrosion [22–25]. However, the structures of these doped polypyrroles at the molecular level and their conductive properties had not been elucidated, so we used DFT to probe the geometric and electronic structures of these chemical systems. This paper reports the results of those investigations.

Models and computational methods

In order to avoid the considerable computational effort that would be required if a full model of polypyrrole were to be investigated, a chain (Fig. 2) containing building blocks of pyrrole was employed for the simulations. This was an oligomer with 5 Py monomers that we denoted ***P***. $(XO_4)^{n-}$ (X = Cl, Mo) anions interact with the second and the fourth pyrrole rings of this chain. The two terminal rings act as chemical media, while the second, third, and fourth rings exhibit properties similar to those of polypyrrole.

All quantum chemical calculations were carried out using DFT. The exchange-correlation energy was calculated using the Perdew, Burke, and Ernzerhof (PBE) nonlocal gradient-corrected functional [44]. The double-zeta plus polarization (DZP) basis set, which is known to be useful for examining hydrogen bonding, was employed for all the atoms. All equilibrium structures were geometrically optimized, applying a threshold for the forces acting on the dynamic atoms of 0.002 Ha/Å.

To our knowledge, no previous DFT-based study of the PPy system has considered the effects of solvent molecules. This is an important oversight, as we would expect the DFT results for electrochemical systems to be significantly influenced by the presence of solvent molecules (H_2O, for instance) [45–47]. In order to take the effects of solvation in water into account, the conductor-like screening model (COSMO) [4] was applied in our study. In this model of continuum solvation, the investigated PPy model was embedded inside a cavity that was demarcated by the solute molecules and characterized by the dielectric continuum of permittivity ε of the solvent.

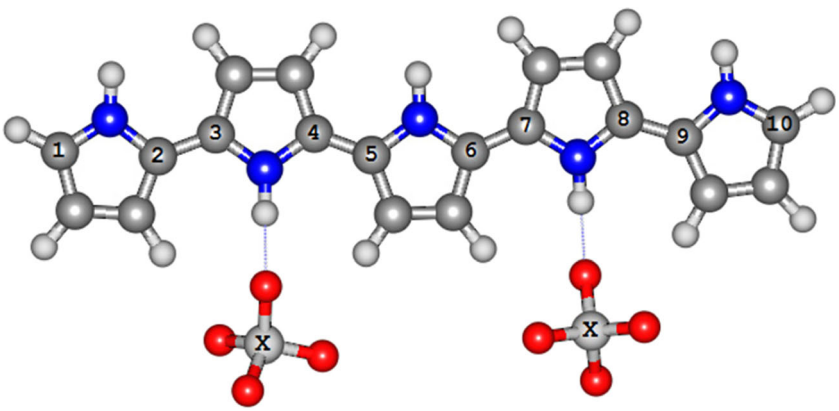

Fig. 2 Model of PPy employed in the study. The *small light-gray balls* represent H atoms, the *darker-gray balls* represent C atoms, the *blue balls* represent N atoms, the *red balls* represent O atoms, and the *gray balls* denoted "X" represent Cl or Mn atoms

Table 1 Bond lengths (in Å) and angles (in degrees) in pyrrole molecule

	C–N	N–H	C–N–C	C–C–N	H–N–C
From theoretical calculations	1.37	1.014	110.00	107.60	125.00
From experiment [49]	1.37	0.996	109.80	107.70	125.10

In order to calculate the band gap energy accurately, a TD-DFT [48] method in which the electron–hole interaction was taken into account was used instead of DFT. The same functional and basis set were used to calculate the energies of the electronic transitions and the oscillator strengths of the transitions (from which UV-Vis absorption spectra were constructed) of all the geometrically optimized models considered in this work. The results of those calculations are presented and discussed in the "Results and discussion" section.

To confirm the accuracy of the computational methods and the models employed here, some evaluations of them were carried out. The first was a comparison between the calculated and experimental geometric parameters (Table 1), which showed that these two sets of data were in fairly good agreement for all bond lengths and bond angles (the maximum error in the N–H bond length was only 1.8%). Secondly, the calculated IR spectrum of ***P***, as shown in Fig. 3, was also found to accurately reproduce the experimental one (obtained from the NIST/EPA Gas-Phase Infrared Database [50]). Because the IR spectrum reflects the structure of the model (i.e., its chemical composition and geometry), the oligomer can be used instead of a full polypyrrole model. However, the calculated electronic energy band gap could not be directly compared to the experimentally determined band gap due to its dependence on the size of the chain: the smaller the chain, the larger the band gap.

Results and discussion

Change in the band gap of PPy after doping

Neutral PPy is an insulator with a band gap of about 3.2 eV, corresponding to an interband transition derived from the π–π* transition of the pyrrole moiety [51]. After oxidation, PPy loses electrons and can be transformed into a semiconductor (oxidized PPy) due to the formation of polaron (a radical cation: a pair of an unpaired electron, •, and a hole with positive charge) and bipolaron states, which function as the charge carriers in PPy.

The presence of anions (A^-) in the PPy stabilizes the chain by neutralizing positive charge. This is demonstrated by the amount of energy released when A^- anions react with oxidized PPy, as shown later in the paper. In addition, the presence of anions can also encourage the pyrrole rings to remain coplanar, which is one condition for achieving a π-conjugated system. The anions can donate negative charge to the oxidized PPy, which can destroy polarons. Two unpaired electrons in two different polarons will combine with each other to form a bipolaron.

When a potential is applied to a doped PPy, π electrons (electrons in $2p_z$ orbitals of carbons in the conjugated system) move towards holes. The disappearance of these π electrons generates other holes. This process occurs continuously, resulting in a current of electrons, implying that the doped PPy is a conductor. Electrons in the HOMO are the easiest ones to detach because these electrons possess the highest energies. The conductivity of PPy depends on both the formation of polarons/bipolarons (when anions are attached to the PPy) and the existence of a conjugated system in the PPy.

Upon the formation of polarons and bipolarons, PPy is transformed into its oxidized form. In this study, we focused on bipolarons of $[\boldsymbol{P}(XO_4)_2]^{n-}$ (X = Cl, Mo; n = 0 and 2) systems, in which PPy has a conventional oxidation state of +2. In order to determine the stable conformations of $[\boldsymbol{P}(ClO_4)_2]^0$ and $[\boldsymbol{P}(MoO_4)_2]^{2-}$ systems, energy optimization was carried out. The results of this indicated that these systems are most stable at an equilibrium state where the anions (ClO_4^- and MoO_4^{2-}) are in contact with the hydrogen atoms of the N–H groups of the second and the fourth pyrrole rings in the PPy chain, as shown in Fig. 4.

For $[\boldsymbol{P}(ClO_4)_2]^0$, the N–H bond is slightly extended (1.03 Å) in comparison to its original value (1.02 Å).

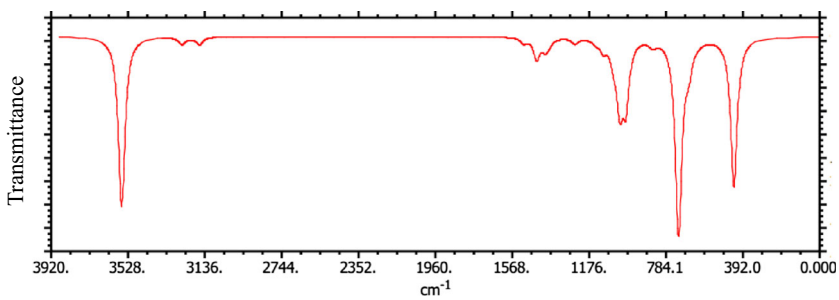

Fig. 3 Calculated IR spectrum of the pyrrole model

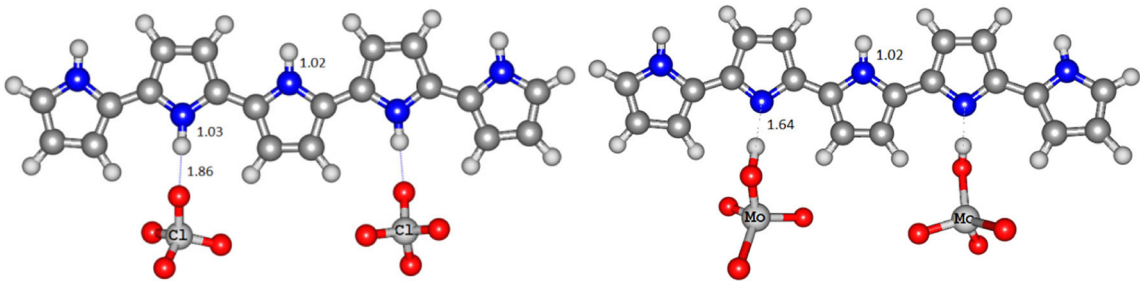

Fig. 4 The $[\boldsymbol{P}(ClO_4)_2]^0$ (*left*) and $[\boldsymbol{P}(MoO_4)_2]^{2-}$ (*right*) systems. The *small light-gray* balls represent H atoms, the *darker-gray balls* represent C atoms, the *blue balls* represent N atoms, the *red balls* represent O atoms, and the *gray balls with chemical symbols* represent Cl and Mn atoms

However, the N–H bond in $[\boldsymbol{P}(MoO_4)_2]^{2-}$ is greatly extended to 1.64 Å; indeed, it breaks completely, leading to the formation of $HMoO_4^-$. This implies that $\boldsymbol{P}^{2+}$ is converted into $\boldsymbol{P}^{1+}$ with the loss of a H^+ or a bipolaron. This means that the interaction between MoO_4^{2-} and PPy is stronger than the interaction between ClO_4^- and PPy, as also demonstrated by the large negative value of the change in the interaction energy (ΔE = −131.49 kJ/mol for MoO_4^{2-} and −55.13 kJ/mol for ClO_4^-).

$$\boldsymbol{P}^{2+} + 2ClO_4^- \rightarrow \left[\boldsymbol{P}(ClO_4)_2\right]^0,\ \Delta E = -55.13\ \text{kJ/mol}$$

$$\boldsymbol{P}^{2+} + 2MoO_4^{2-} \rightarrow \left[\boldsymbol{P}(MoO_4)_2\right]^{2-},\ \Delta E = -131.49\ \text{kJ/mol}$$

According to the results of the optimization process, the $[\boldsymbol{P}(MoO_4)_2]^{2-}$ and $\boldsymbol{P}(ClO_4)_2]^0$ systems are both flat and therefore can readily adopt conjugated structures. As mentioned above, values of the band gap energy (E_g) obtained from TD-DFT calculations for conformations of $[\boldsymbol{P}(MoO_4)_2]^{2-}$ and $\boldsymbol{P}(ClO_4)_2]^0$ in their equilibrium states represent the difference between the HOMO and LUMO. The magnitude of the oscillator strength (f) determines the transferability of an electron from the HOMO to the LUMO, and can be expressed as follows [52, 53]:

$$f_{H\rightarrow L} = \frac{2m_e}{3\hbar^2}(E_L - E_H)\sum_{\alpha=x,y,z}|\Psi_H|R_\alpha|\Psi_L|^2 \qquad (1)$$

Table 2 Values of the band gap energy (E_g, in eV) and the oscillator strength for the transfer of an electron from the HOMO to the LUMO (f, in arbitrary units) for the studied systems

$\boldsymbol{P}^0$	$\boldsymbol{P}^0$	$[\boldsymbol{P}(ClO_4)_2]^{2-}$	$[\boldsymbol{P}(MoO_4)_2]^{4-}$
E_g/f	2.79/1.23	2.78/1.17	2.78/1.01
$\boldsymbol{P}^{2+}$	Free $\boldsymbol{P}^{2+}$	$[\boldsymbol{P}(ClO_4)_2]^0$	$[\boldsymbol{P}(MoO_4)_2]^{2-}$
E_g/f	1.83/1.67	1.81/1.66	1.71/1.21
$\boldsymbol{P}^{4+}$	Free $\boldsymbol{P}^{4+}$	$[\boldsymbol{P}(ClO_4)_2]^{2+}$	$[\boldsymbol{P}(MoO_4)_2]^0$
E_g/f	1.79/0.00	0.68/0.00	0.63/0.02

Here, the subscripts L and H refer to the LUMO and HOMO, respectively. The operator R_x is the sum of the x-coordinates $r_{i,x}$ of all N electrons in the system:

$$R_\alpha = \sum_{i=1}^{N} r_{i,\alpha} \qquad (2)$$

Based on the results shown in Table 2, we can draw the following conclusions:

(i) If ClO_4^- or MoO_4^{2-} is added to neutral PPy ($\boldsymbol{P}^0$), the band gap energy barely changes (to 2.78 eV for $[\boldsymbol{P}(XO_4)_2]^{n-}$; it is 2.79 eV for $\boldsymbol{P}^0$). Therefore, it is necessary to oxidize the PPy before doping with ClO_4^- or MoO_4^{2-} anions to achieve a highly conductive polymer.

(ii) The band gap energy of the oxidized PPy (free $\boldsymbol{P}^{2+}$ and $\boldsymbol{P}^{4+}$, or those species within anions) is significantly lower than that of $\boldsymbol{P}^0$. Oxidation therefore converts PPy into a low band gap polymer (E_g < 2.0 eV).

(iii) The presence of ClO_4^- or MoO_4^{2-} in PPy barely alters the band gap energy and oscillator strength of $\boldsymbol{P}^{2+}$.

(iv) If the oxidation state of PPy is greater than +2, as in $\boldsymbol{P}^{4+}$, there is no transfer of an electron from the HOMO to the LUMO because the oscillator strength is approximately zero. Though the addition of ClO_4^- or MoO_4^{2-} to $\boldsymbol{P}^{4+}$ lowers its band gap, there is no electron transfer from the HOMO to the LUMO. This result implies that the conductivity of the polymer depends mainly on the ratio of oxidized PPy (containing $\boldsymbol{P}^{2+}$ or $\boldsymbol{P}^{4+}$) to neutral PPy. In this study, we employed a ratio of 2/5 in our calculations and obtained results that were in good agreement with the above hypothesis about the formation of bipolarons.

In addition, the computed charges on the carbon atoms in free $\boldsymbol{P}^{2+}$ indicated that the charges on the carbon atoms near nitrogen atoms were more positive than those on other carbon atoms, as shown in Fig. 5. However, the third and eighth carbon atoms (circled in Fig. 5) had the highest positive charges. These positions coincide with the positions of bipolaron holes.

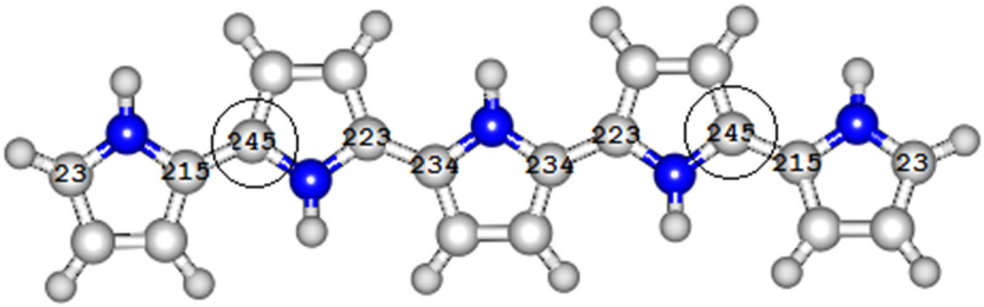

Fig. 5 Positive charges ($\times 10^3$) on carbon atoms next to nitrogen atoms in free P^{2+}

In Fig. 6, it is apparent that the electron density around the third and eighth carbon atoms of free P^{2+} is too low to discern (using an isovalue of 0.03 e/Å^3), which means that the positive charges on these two atoms are large, as can be seen in Fig. 5. However, this behavior was not seen for the neutral PPy. The oxidative addition of ClO_4^- or MoO_4^{2-} decreases the E_g value of PPy from 2.80 eV to 1.81 eV or 1.71 eV, respectively. These values of E_g are characteristic of semiconductors (for example, the band gap energies of CdSe and CdS are 1.73 and 2.42 eV, respectively) [54].

Electronic spectroscopy

In general, the electronic structure of a conducting polymer can be used to derive important information about the optical spectrum of the polymer, and vice versa. The conjugation present in

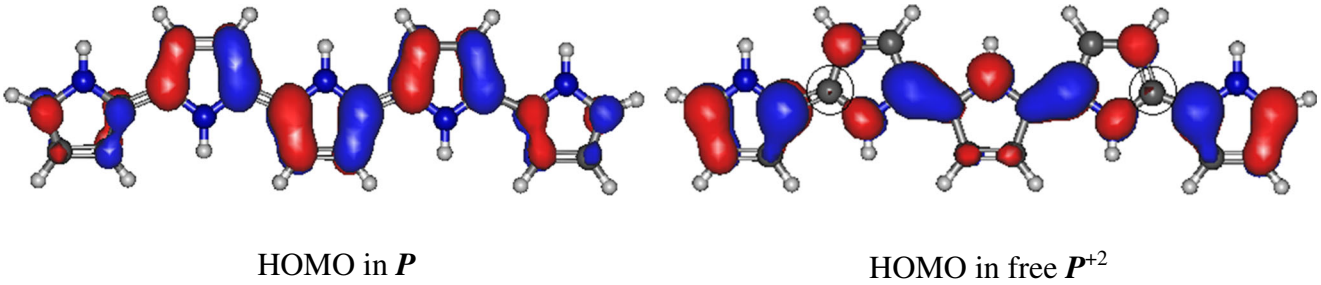

Fig. 6 The HOMOs in P (*left figure*) and P^{2+} (*right figure*) (plotted at an isovalue of 0.03 e/Å^3)

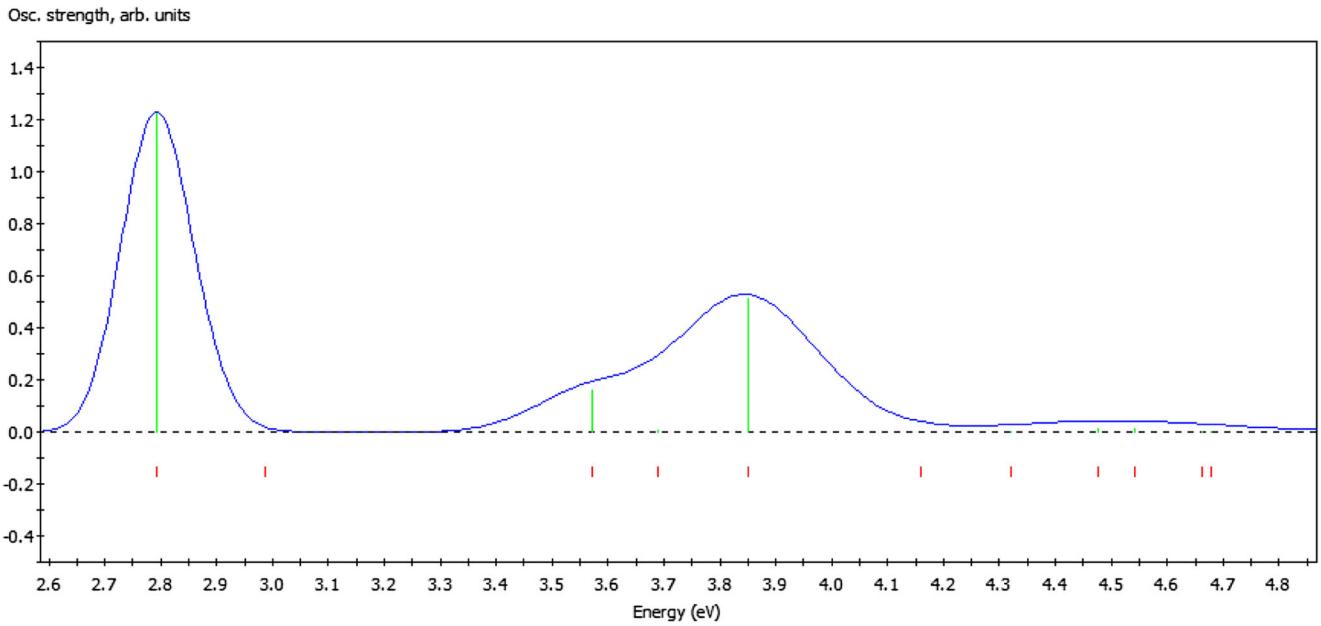

Fig. 7 Electronic spectroscopy of PPy. The first absorption band (centered at 2.79 eV) corresponds to electron transfer from the HOMO to the LUMO, while the second band (centered at 3.85 eV) is due to electron transfer from the HOMO-1 to the LUMO+1

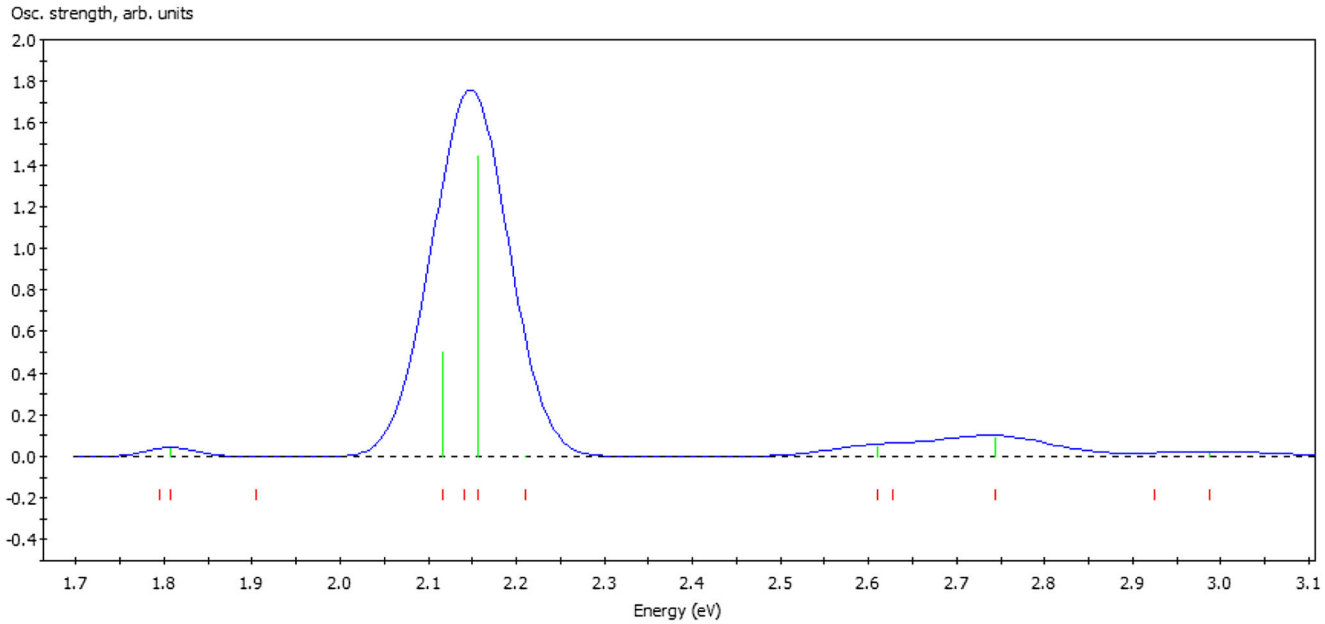

Fig. 8 Electronic spectroscopy of free $\boldsymbol{P}^{4+}$. The absorption band at 2.16 eV corresponds to electron transitions from the HOMO-4 to the LUMO

a PPy chain determines its color, so the optical spectrum of the polymer is needed to characterize the electronic processes that take place in the PPy chain during doping. The changes that occur to the optical spectrum of the PPy chain upon doping can be analyzed in order to elucidate the mechanism for the doping process and the charge distribution in the PPy.

Figure 7 shows the UV-Vis spectrum of PPy as a plot of excitation energy against oscillator strength (in arbitrary units). Two important peaks can be seen at excitation energies of 2.79 and 3.85 eV. The sharp peak at 2.79 eV was assigned to electron transfer from the HOMO to the LUMO, while the broad peak at 3.85 eV was assigned to electron transfer from the HOMO-1 to the LUMO+1.

The UV-Vis spectrum of $\boldsymbol{P}^{2+}$ is similar to that of PPy ($\boldsymbol{P}^{0}$), but the sharp peak corresponding to electron transfer from the HOMO to the LUMO is shifted into the infrared region and its intensity increases from 1.23 to 1.67. Meanwhile, the broad peak is assigned to electron transfer from the HOMO to the LUMO+2, and it decreases in intensity from 0.52 to 0.32 for $\boldsymbol{P}^{2+}$, though it also shifts into the infrared region.

According to the calculations, the UV-Vis spectra of $[\boldsymbol{P}(ClO_4)_2]^0$ and $[\boldsymbol{P}(MoO_4)_2]^{2-}$ have the same shape as the spectrum of PPy. Although the most intense peaks of these spectra were assigned to electron transfer from the HOMO to the LUMO, the spectra vary in the positions and intensities of the peaks. In the case of $[\boldsymbol{P}(ClO_4)_2]^0$, there is no broad peak. The shapes of the HOMOs and LUMOs of $[\boldsymbol{P}(ClO_4)_2]^0$ and $[\boldsymbol{P}(MoO_4)_2]^{2-}$ are similar to those of free PPy^{2+} without contributions from the ClO_4^- or MoO_4^{2-} anions. This reveals that the formation of a conducting polymer from PPy does not depend on the nature of the oxidant; the only requirement is that the oxidant converts PPy into a suitable oxidized form, such as PPy^{2+}.

The calculated UV-Vis spectrum of free $\boldsymbol{P}^{4+}$ (see Fig. 8) has just one major peak, at about 2.16 eV, which was assigned to electron transfer from the HOMO-4 to the LUMO. It is interesting that no such peak is seen for $[\boldsymbol{P}(ClO_4)_2]^{2+}$ and $[\boldsymbol{P}(MoO_4)_2]^0$. An analysis of the HOMO, HOMO-1, HOMO-2, … up to the HOMO-6 showed that there is no conjugation in the polymer chain; if this is also the case for PPy, the oxidized form PPy^{4+} will not conduct.

Conclusions

(1) This study has demonstrated the existence of a bipolaron in the ($-Py^+-Py-Py^+-$) system.
(2) In order to convert PPy into a conducting polymer, the PPy must be carefully oxidized to get polarons or bipolarons. Further oxidation could diminish the conductivity of the polymer.
(3) The conversion of PPy into a conducting polymer does not depend on the nature of the oxidant used, provided that it can convert PPy into a suitable oxidized form containing polarons/bipolarons. In this form, the conductivity of PPy is barely influenced by the presence of counter anions such as ClO_4^- [55]. However, if an anion shows a very strong affinity for H^+ (e.g., MoO_4^-), its presence may reduce the conductivity of the PPy.

Acknowledgements This research was funded by the Vietnam National Foundation for Science and Technology Development (NAFOSTED) under grant number 104.02-2013.69.

References

1. Diaz AF, Kanazawa KK, Gardini GP (1979) Electrochemical polymerization of pyrrole. J Chem Soc Chem Commun 14:635–646. https://doi.org/10.1039/C39790000635
2. Fonner JM, Schmidt CE, Ren P (2010) A combined molecular dynamics and experimental study of doped polypyrrole. Polymer 51:4985–4993. https://doi.org/10.1016/j.polymer.2010.08.024
3. Diaz AF, Bargon J (1986) In: Skotheim TA (ed) Handbook of conducting polymers, vol. 1. Marcel Dekker, New York, p. 82
4. Ouyang J, Li Y (1997) Great improvement of polypyrrole films prepared electrochemically from aqueous solutions by adding nonaphenolpolyethyleneoxy (10) ether. Polymer 38:3997–3999. https://doi.org/10.1016/S0032-3861(97)00087-6
5. Myers RE (1986) Chemical oxidative polymerization as a synthetic route to electrically conducting polypyrroles. J Electron Mater 15: 61–69. https://doi.org/10.1007/BF02649904
6. Armes SP (1987) Optimum reaction conditions for the polymerization of pyrrole by iron(III) chloride in aqueous solution. Synth Met 20:365–371. https://doi.org/10.1016/0379-6779(87)90833-2
7. Dai Y, Wei C, Blaisten-Barojas E (2013) Density functional theory study of neutral and oxidized thiophene oligomers. J Chem Phys 139:184905. https://doi.org/10.1063/1.4829538
8. Barford W, Marcus M, Tozer OR (2016) Polarons in π-conjugated polymers: Anderson or Landau? J Phys Chem A 120:615–620. https://doi.org/10.1021/acs.jpca.5b08764
9. Deibel C, Strobel T, Dyakonov V (2009) Origin of the efficient polaron-pair dissociation in polymer-fullerene blends. Phys Rev Lett 103:036402. https://doi.org/10.1103/PhysRevLett.103.036402
10. Kowalski D, Ueda M, Ohtsuka T (2007) The effect of counter ions on corrosion resistance of steel covered by bi-layered polypyrrole film. Corros Sci 49:3442–3452. https://doi.org/10.1016/j.corsci.2007.03.007
11. Johanson U, Marandi M, Tamm T, Tamm J (2005) Comparative study of the behavior of anions in polypyrrole films. Electrochim Acta 50(7–8):1523–1528. https://doi.org/10.1016/j.electacta.2004.10.016
12. Zhou X, Chen X, He T, Bi Q, Sun L, Liu Z (2017) Fabrication of polypyrrole/vanadium oxide nanotube composite with enhanced electrochemical performance as cathode in rechargeable batteries. Appl Surf Sci 405(31):146–151. https://doi.org/10.1016/j.apsusc.2017.02.050
13. Fang W, Zhang N, Fan L, Sun K (2017) Preparation of polypyrrole-coated Bi_2O_3@CMK-3 nanocomposite for electrochemical lithium storage. Electrochim Acta 238(1):202–209. https://doi.org/10.1016/j.electacta.2017.04.032
14. Shrestha AR, Shrestha S, Park CH, Kim CS (2017) In situ synthesis of cylindrical spongy polypyrrole doped protonated graphitic carbon nitride for cholesterol sensing application. Biosens Bioelectron 94:686–693. https://doi.org/10.1016/j.bios.2017.03.072
15. Ayenimo JG, Adeloju SB (2017) Amperometric detection of glucose in fruit juices with polypyrrole-based biosensor with an integrated permselective layer for exclusion of interferences. Food Chem 229:127–135. https://doi.org/10.1016/j.foodchem.2017.01.138
16. Afzal A, Abuilaiwi FA, Habib A, Awais M, Waje SB, Atieh MA (2017) Polypyrrole/carbon nanotube supercapacitors: technological advances and challenges. J Power Sources 352:174–186. https://doi.org/10.1016/j.jpowsour.2017.03.128
17. Fang Y, Jiang X, Niu L, Wang S (2017) Constructing polypyrrole/aligned carbon nanotubes composite materials as electrodes for high-performance supercapacitors. Mater Lett 190:232–235. https://doi.org/10.1016/j.matlet.2016.12.110
18. Ebrahimi I, Gashti MP (2016) Chemically reduced versus photo-reduced clay-Ag-polypyrrole ternary nanocomposites: comparing thermal, optical, electrical and electromagnetic shielding properties. Mater Res Bull 83:96–107. https://doi.org/10.1016/j.materresbull.2016.05.024
19. Zhao HL, Lu Y (2016) Electromagnetic shieldingeffectiveness and serviceability of the multilayer structured cuprammonium fabric/polypyrrole/copper (CF/PPy/Cu) composite. Chem Eng J 297: 170–179. https://doi.org/10.1016/j.cej.2016.04.004
20. Grari O, Taouil AE, Dhouibi L, Buron CC, Lallemand F (2015) Multilayered polypyrrole SiO_2 composite coatings for functionalization of stainless steel: characterization and corrosion protection behavior. Prog Org Coat 88:48–53. https://doi.org/10.1016/j.porgcoat.2015.06.019
21. Vera R, Schrebler GP, Romero H (2014) The corrosion-inhibiting effect of polypyrrole films doped with *p*-toluene-sulfonate, benzene-sulfonate or dodecyl-sulfate anions, as coating on stainless steel in NaCl aqueous solutions. Prog Org Coat 77(4):853–858. https://doi.org/10.1016/j.porgcoat.2014.01.015
22. Paliwoda-Porebska G, Rohwerder M, Stratmann M, Rammelt U, Duc LM, Plieth W (2006) Release mechanism of electrodeposited polypyrrole doped with corrosion inhibitor anions. J Solid State Electrochem 10(9):730–736. https://doi.org/10.1007/s10008-006-0118-y
23. Rammelt U, Duc LM, Plieth W (2005) Improvement of protection performance of polypyrrole by dopant anion. J Appl Electrochem 35:1225–1230. https://doi.org/10.1007/s10800-005-9033-7.
24. Trung VQ, Hoan PV, Phung DQ, Duc LM, Hang LTT (2014) Double corrosion protection mechanism of molybdate-doped polypyrrole/montmorillonite nanocomposites. J Exp Nanosci 9(3): 282–292. https://doi.org/10.1080/17458080.2012.656710
25. Ilangovan G, Pillai KC (1999) Preparation and characterisation of monomeric molybdate(VI) anion-doped polypyrrole electrodes. J Solid State Electrochem 3(7):474–477. https://doi.org/10.1007/s100080050184
26. Klamt A, Schüürmann G (1993) COSMO: a new approach to dielectric screening in solvents with explicit expressions for the screening energy and its gradient. J Chem Soc Perkin Trans 2(5): 799–805. https://doi.org/10.1039/P29930000799
27. Hoang HV, Nguyen TD, Nguyen HN (2013) Corrosion inhibition mechanism of pyridine ion iron and its alloys using DFT. Asian J Chem 25(6):3117–3120. 10.14233/ajchem.2013.13548
28. Li WK, Hu P, Lu G, Gong XQ (2014) Density functional theory study of mixed-phase TiO_2: heterostructures and electronic properties. J Mol Model 20(4):2215. https://doi.org/10.1007/s00894-014-2215-7.
29. Supatutkul C, Pramchu S, Jaroenjittichai AP, Laosiritawor Y (2016) Density functional theory investigation of surface defects in Sn-doped ZnO. Surf Coat Technol 306(Pt A):364–368. https://doi.org/10.1016/j.surfcoat.2016.04.013
30. Sun J, Xie X, Cao B, Duan H (2017) A density functional theory study of Au_{13}, Pt_{13}, $Au_{12}Pt$ and $Pt_{12}Au$ clusters. Comput Theor Chem 1107:127–135. https://doi.org/10.1016/j.comptc.2017.02.002
31. Rad AS, Esfahanian M, Ganjian E, Tayebi H, Novir SB (2016) Thepolythiophene molecular segment as a sensor model for H_2O, HCN, NH_3, SO_3, and H_2S: a density functional theory study. J Mol Model 22(6):127. https://doi.org/10.1007/s00894-016-3001-5.
32. Asath RM, Rekha TN, Premkumar S, Mathavan T, Benial AMF (2016) Vibrational, spectroscopic, molecular docking anddensity functional theory studies on *N*-(5-aminopyridin-2-yl)acetamide. J Mol Struct 1125:633–642. https://doi.org/10.1016/j.molstruc.2016.07.064
33. Jomphoak A, Maezono R, Onjun T (2016) Density functional theory, of graphene/Cu phthalocyanine composite material. Surf Coat Technol 306(Pt A):236–239. https://doi.org/10.1016/j.surfcoat.2016.06.015

34. López-Carballeira D, Ruipérez F (2016) Evaluation of modern DFT functionals and G3n-RAD composite methods in the modelization of organic singlet diradicals. J Mol Model 22(4):76. https://doi.org/10.1007/s00894-016-2950-z.
35. Dai Y, Chowdhury S, Blaisten-Balojas E (2011) Density functional theory study of the structure energetics of negatively charged oligopyrroles. Int J Quantum Chem 111:2295–2305. https://doi.org/10.1002/qua.22659
36. Ullah H, ShahA u-H A, Bilal S, Ayub K (2014) Doping and dedoping processes of polypyrrole: DFT study with hybrid functionals. J Phys Chem C 118(31):17819–17830. https://doi.org/10.1021/jp505626d
37. Abdulla HS, Abbo AI (2012) Optical and electrical properties of thin films of polyaniline and polypyrrole. Int J Electrochem Sci 7:10666–10678
38. Ullah R, Ullah H, Shah A-u-H A, Bilal S, Ali K (2017) Oligomeric synthesis and density functional theory of leucoemeraldine base form of polyaniline. J Mol Struct 1127:734–741. https://doi.org/10.1016/j.molstruc.2016.08.009
39. Zhang Y, Duan Y, Liu J (2017) Time-dependent density functional theory study on the excited-state hydrogen-bonding characteristics of polyaniline in aqueous environment. Spectrochim Acta A 171:305–310. https://doi.org/10.1016/j.saa.2016.08.039
40. Cherrak Z, Lagant P, Benharrats N, Semmoud A, Hamdache F, Vergoten G (2005) Density functional theory and empirical derived force fields for the delocalized polaron form of polyaniline: application to properties determination of an isolated oligomer using molecular dynamics simulations. Spectrochim Acta A 61(7):1419–1429. https://doi.org/10.1016/j.saa.2004.10.046
41. Rittmeyer SP, Groß A (2012) Structural and electronic properties of oligo- and polythiophenes modified by substituents. Beilstein J Nanotechnol 3:909–919. https://doi.org/10.3762/bjnano.3.101
42. Ramírez-Solís A, Kirtman B, Bernal-Jáquez R, Zicovich-Wilson CM (2009) Periodic density functional theory studies of Li-doped polythiophene: dependence of electronic and structural properties on dopant concentration. J Chem Phys 130:164904. https://doi.org/10.1063/1.3109079
43. Bouzzine SM, Salgado-Morán G, Hamidi M, Bouachrine M, Pacheco AG, Glossman-Mitnik D (2015) DFT study of polythiophene energy band gap and substitution effects. J Chemistry 296386. https://doi.org/10.1155/2015/296386.
44. Perdew JP, Burke K, Ernzerhof (1996) Generalized gradient approximation made simple. Phys Rev Lett 77:3865–3868. https://doi.org/10.1103/PhysRevLett.77.3865
45. Yurtsever E, Yurtsever M (1999) A theoretical study of structural defects in conjugated polymers. Synth Met 101(1–3):335–336. https://doi.org/10.1016/S0379-6779(98)01343-5
46. Rabias I, Howlin BJ (2001) A combined ab initio and semi-empirical study on the theoretical vibrational spectra and physical properties of polypyrrole. Comput Theor Polym Sci 11:241–249. https://doi.org/10.1016/S1089-3156(00)00010-6
47. Santos MJL, Rubira AF, Pontes RM, Basso EA, Girotto EM (2006) Electrochromic properties of poly(alkoxy-terthiophenes): an experimental and theoretical investigation. J Solid State Electrochem 10:117–122. https://doi.org/10.1007/s10008-005-0679-1
48. Runge E, Gross EKU (1984) Density-functional theory for time-dependent systems. Phys Rev Lett 52(12):997–1000. https://doi.org/10.1103/PhysRevLett.52.997
49. Nygaard U, Nielsen JT, Kirchheiner J, Maltesen G, Rastrup-Andersen J, Sørensen GO (1969) Microwave spectra of isotopic pyrroles. Molecular structure, dipole moment, and ^{14}N quadrupole coupling constants of pyrrole. J Mol Struct 3(6):491–506. https://doi.org/10.1016/0022-2860(69)80031-1
50. NIST (2017) NIST Standard Reference Database 35: NIST/EPA Gas-Phase Infrared Database JCAMP Format. https://www.nist.gov/srd/nist-standard-reference-database-35.
51. Jones RA, Bean GP (1977) Chemistry of pyrroles. Academic, New York
52. Hilborn RC (1982) Einstein coefficients, cross sections, f values, dipole moments, and all that. Am J Phys 50:982–986. https://doi.org/10.1119/1.12937.
53. Hilborn RC (1983) Erratum: "Einstein coefficients, cross sections, f values, dipole moments, and all that". Am J Phys 51(5):471. https://doi.org/10.1119/1.13515
54. Streetman BG, Banerjee S (2000) Solid state electronic devices, 5th edn. Prentice Hall, Upper Saddle River
55. Wencheng S, Iroh JO (2000) Electrodeposition mechanism of polypyrrole coatings on steel substrates from aqueous oxalate solutions. Electrochim Acta 46(1):1–8. https://doi.org/10.1016/S0013-4686(00)00518-1